THE JOURNAL OF PHYSICAL CHEMISTRY B
A JOURNAL OF THE AMERICAN CHEMICAL SOCIETY

pubs.acs.org/JPCB

Article

Stability of a Monoethanolamine-CO_2 Zwitterion at the Vapor/Liquid Water Interface: Implications for Low Partial Pressure Carbon Capture Technologies

Alessandro Sinopoli, Ahmed Abotaleb, Fabio Pietrucci, and Ivan Gladich*

Cite This: *J. Phys. Chem. B* 2021, 125, 4890−4897

Read Online

ACCESS | Metrics & More | Article Recommendations | Supporting Information

ABSTRACT: The need to chemically convert CO_2 at the interface of aqueous amine solutions has become particularly relevant for the development and the broad distribution of cost-effective and near-future devices for direct air capture working at low (e.g., ambient) partial pressure. Here, we have determined the stability of a CO_2-monoethanolamine zwitterion and its chemical conversion into carbamate at the vapor/liquid water interface by first-principles molecular dynamics simulations coupled with a recently introduced enhanced sampling technique. Contrary to the bulk water case, our results show that both the zwitterion and carbamate ions are poorly stable at the vapor/amine aqueous interface, further stating the differences between the homogeneous and heterogeneous CO_2 chemical conversion. The design of novel and cost-effective capture systems, such as those offered by amine-based scrubbing solutions, working at low (e.g., ambient) CO_2 partial pressure should explore the use of novel solvents, different from aqueous mixtures, to overcome the limits of the current absorbents.

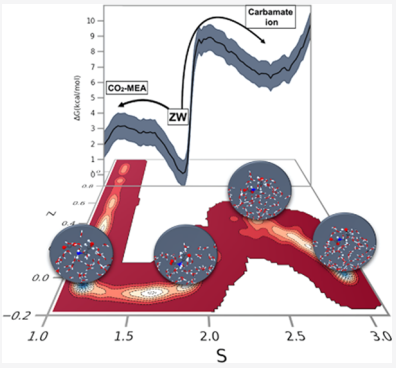

INTRODUCTION

Carbon Capture and Utilization (CCU) represents one of the most promising CO_2-based technologies[1] aiming to mitigate the impact of CO_2 greenhouse gas on climate change while converting carbon dioxide into added-value products/chemicals.[2,3] CO_2 is the main product of fuel combustion, and removal from flue gas is traditionally done with amine-based scrubbing solutions. (Apolar) gas-phase CO_2 is chemically absorbed by amines as carbamate or bicarbonate ions.[4−7] These species are more soluble in polar solvents and play a key role in the CO_2 conversion processes. Despite the large basic and applied research interest, the regeneration of amine-based scrubbers remains an energetically expensive step.[8−10] Therefore, this process stays in the industrial sector, where typically high CO_2 partial pressures are needed to solvate CO_2 gas into polar amine scrubbing solutions, enabling cost-effective capturing and eventually conversion. Interestingly, the need to capture and convert CO_2 even at low loading/partial pressure has become particularly relevant for the development of new technologies, which could also enable the widespread distribution in the near future of direct air capture devices.[11−13]

We have recently demonstrated[14] that the initial CO_2 capture occurs in heterogeneous environments, i.e., at the gas/amine solution interface, by the formation of a stable and interfacial CO_2-amine precomplex. From this interfacial precomplex, one of the chemical channels for carbon dioxide capture/conversion proceeds toward the formation of a zwitterionic CO_2-amine intermediate (hereafter, ZW) and, from that, to carbamate (i.e., a negatively charged ion obtained by the release of one of the two protons from the amino group of ZW). Figure 1 displays the zwitterionic pathway for CO_2 capture in a monoethanolamine aqueous solution. The interfacial capture occurs at both low and high CO_2 concentrations in solution, but it is especially relevant at lower ones due to the low CO_2 partial pressure. The stability of ZW in bulk aqueous solution, which concerns high CO_2

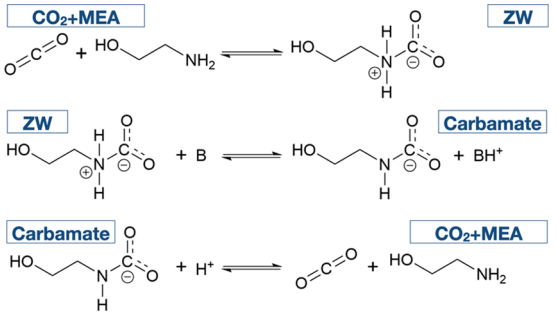

Figure 1. MEA and CO_2 zwitterionic reaction mechanism.

Received: February 24, 2021
Revised: April 7, 2021
Published: April 22, 2021

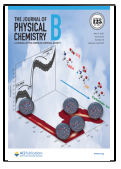

https://doi.org/10.1021/acs.jpcb.1c01661
J. Phys. Chem. B 2021, 125, 4890−4897

loading/partial pressure systems, has been studied by first-principles MD (FPMD) simulations[15−17] or by quantum chemical calculations of the enthalpic reaction profile in implicit or implicit/explicit hybrid solvent models.[5,18−20] To the best of our knowledge, the stability of the ZW at the interface is still unknown.

In this paper, we investigated the stability of the CO_2-monoethanolamine (MEA) zwitterion and its chemical conversion into carbamate at the vapor/liquid water interface by first-principles molecular dynamics coupled with enhanced sampling techniques, including a novel free-energy method based on a topological metric.[21] MEA aqueous solutions are considered as a benchmark for the amine scrubbing solutions,[22] and, for this reason, the atomic structure and the dynamical properties of the bulk (but not of the interface) of the solution have been well characterized experimentally and by molecular dynamics.[22−27] Our results show that the ZW corresponds to a free-energy minimum structure at the interface, but it is poorly stable, with a free-energy barrier to dissociate CO_2 from MEA of ∼3 kcal/mol. Moreover, ZW conversion into carbamate is hampered by a free-energy barrier of ∼9 kcal/mol, while the formation of ZW from carbamate has a barrier of only 2 kcal/mol. Compared to the ZW in bulk water, interfacial ZW is less stable: this is ascribed to the (∼half) solvation shell around the interfacial ZW, which results in smaller enthalpic and entropic costs for the CO_2 release in the gas phase by the ZW dissociation. The results of this work indicate the poor stability of ZW and carbamate at the interface of aqueous amine solutions.

Altogether, this work suggests that the use of novel solvents, different from aqueous mixtures, is strongly recommended to overcome the limits of the current absorbents: preliminary experimental studies in organic solvents seem to point in that direction.[28,29] This is particularly relevant for the potential design of novel and cost-effective capture systems at ambient and low CO_2 partial pressure[11−13] in which the capture process is extremely likely to occur at the interface of the scrubbing solution. Finally, the computational approach adopted here, which employs a novel topological metric for the exploration of the free-energy pathways, enables a more exhaustive description of all reaction intermediates while feasibly addressing interfacial processes that are otherwise hardly accessible experimentally or that are computationally costly by first-principles-based standard simulations.

METHODS

All of the molecular dynamics (MD) simulations were performed at the first-principles level, i.e., the forces driving the dynamics were calculated "on-the-fly" based on density functional theory.[30] First-principles MD (FPMD) simulations were carried out using the CP2K molecular dynamics package[31] and the Gaussian and Plane Waves (GPW) method implemented in CP2K. The BLYP[32,33] density functional with Grimme dispersion correction (D3)[34] was adopted. The DZVP basis set level was used for valence electrons, while core electrons were treated by Goedecker−Teter−Hutter pseudopotentials.[35] The cutoff was set to 400 Ry. The temperature was kept at 300 K using a Langevin thermostat[36] and a time constant of 300 fs. The time step was set to 0.5 fs. This (or very similar) computational setup has been extensively used in the literature for simulations of bulk water and vapor/liquid water interfaces,[37−39] while the reliability of our DFT functional choice has been previously tested for CO_2 capture and release by MEA in bulk aqueous solution.[15,16] Further computational details are reported in the Supporting Information (SI).

A liquid water box of 216 water molecules and the initial dimension of ∼15 × 15 × 32 $Å^3$ was equilibrated at 1 bar pressure and 300 K using classical MD and the TIP3P water model.[40] The equilibration protocol at classical MD is reported elsewhere.[41,42] After the equilibration at classical MD, the *Z*-dimension of the simulation box was enlarged to 72 Å, resulting in a water slab system with two vapor/liquid water interfaces. The monoethanolamine-CO_2 zwitterion (ZW) was placed on the top of one of the two interfaces, and the system was geometrically optimized at the BLYP-D3 level. The optimized structure was the starting configuration for the FPMD production run at constant volume and temperature (NVT).

PLUMED plug-in[43] was used to combine our FPMD simulations with enhanced sampling methods (i.e., metadynamics and umbrella sampling) to determine the stability of the ZW and its chemical conversion at the interface. Two different sets of two reaction coordinates (also called collective variables, CVs) were employed. First, we used the distance (N−C) between the nitrogen atom of MEA, N_{MEA}, and the carbon atom of CO_2 and the coordination number between N_{MEA} and the two hydrogens of the amine group. The coordination number (CN) of N_{MEA} with the two amine hydrogen atoms was considered to describe the deprotonation of the amine group and the conversion of the ZW into a carbamate ion. The CN is constructed by employing a switching function of the atomic distance: when both hydrogens are bounded to N_{MEA}, CN ∼ 1.6−1.8, when N_{MEA} deprotonates one hydrogen, CN drops to half of the value, i.e., CN ∼ 0.8−0.9. Figure S1 provides a visual inspection of these two CVs. For the second set of coordinates, the *S*,*Z* path reaction coordinates were adopted. The metric in the *S*,*Z* space was based on a recently introduced topological distance,[21] defined from the set of coordination numbers among different groups of atoms in the system,[21,44] i.e., between (a) the N_{MEA} and the C_{CO_2}, (b) the carboxylic oxygens and all of the hydrogens, Hs, in the system, (c) N_{MEA} and Hs, and (d) C_{CO_2} and the oxygen of the alcoholic tail. This last coordination was introduced to evaluate a possible attack of CO_2 on the alcoholic tail rather than on the amine group. A full description of the reaction coordinates and of the computational details for the metadynamics and umbrella sampling runs is reported, including input files, in the SI.

RESULTS AND DISCUSSION

Figure 2 shows a 10 ps FPMD simulation for the ZW initially located at the vapor/liquid water interface (Figure 2a). Figure 2b displays the water oxygen profile in red, indicating two interfacial environments at about z ±1 nm. The ZW is initially stable and resides in that interfacial environment, as shown by the z-coordinate for the carbon atom of CO_2 (C_{CO_2}) and the nitrogen atom of MEA (N_{MEA}) reported as black and blue horizontal lines in Figure 2b, respectively. In the first 4.5 ps, the N_{MEA}−C_{CO_2} bond distance is 0.16 ± 0.01 nm. After 4.5 ps, the CO_2 is released from the ZW and CO_2 structurally converts from a bent into a linear geometry, as shown in the inset of Figure 2b. Interestingly, the black line in Figure 2b indicates a slight but constant increase of the CO_2 z-coordinate

https://doi.org/10.1021/acs.jpcb.1c01661
J. Phys. Chem. B 2021, 125, 4890−4897

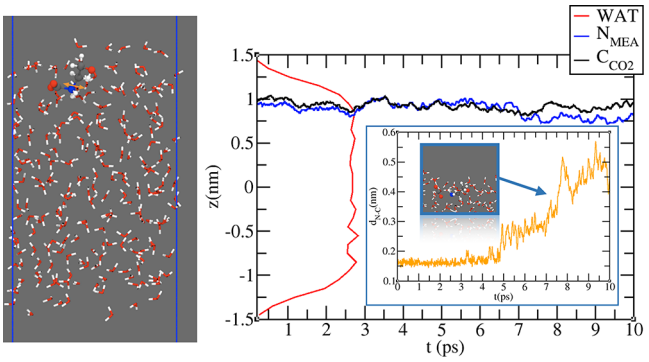

Figure 2. FPMD simulation of ZW at the vapor/liquid water interface. (a) Starting configuration of the 10 ps FPMD simulation. (b) Probability density profile, n_i/n_{tot}, normalized to the unity for the water oxygen as a function of the z-coordinate perpendicular to the air/liquid water interface (in red). The horizontal black and blue lines are the z-coordinates as a function of time of the C_{CO_2} and N_{MEA}, respectively. In the blue inset, the C_{CO_2}–N_{MEA} distance as a function of time is given. Atom color code: C (gray), H (white), O (red), N (blue). The CO_2 and MEA molecules are shown in ball and stick representation.

after 7 ps, suggesting that carbon dioxide starts moving outward after the dissociation, as a result of the fact that linear CO_2 is apolar and poorly soluble in a (polar) amine aqueous solution.

To determine the free-energy landscape governing the interfacial stability of the ZW and its chemical conversion into a carbamate ion or its dissociation into MEA and CO_2, we coupled our FPMD simulations with enhanced sampling techniques. In Figure 3a is depicted the 2D bias surface in the N–C and CN space obtained from a 29 ps long metadynamics[45] run. The metadynamics trajectories show the initial ZW (back and forward) deprotonation and conversion into carbamate after ∼1.3 ps. At 4 ps, CO_2 dissociates from the ZW to recombine again in ZW at 7.8 ps. At 8.5 ps, the formation of carbamic acid is observed. Another CO_2 dissociation (recombination) from (to) the ZW is observed at 17 ps (21 ps). Due to the lack of multiple recrossings among minima, this initial metadynamics run provides only an approximate picture of the free-energy landscape, but it enables the identification of the relevant pathways and intermediate states and, from that, the sampling of statistically converged 1D free-energy profiles by umbrella sampling.[46] Figure 3b shows the latter 1D profiles with the ZW (N–C = ∼0.16 nm, CN = ∼1.7) and carbamate ion (N–C = ∼0.15 nm, CN = ∼0.9) lying at comparable free-energy levels in the landscape. Figure 3b also shows a ZW-to-carbamate barrier of about 7 kcal/mol located at CN = ∼1.2 and a ZW dissociation barrier to CO_2 and MEA of ∼4 kcal/mol at N–C = ∼0.22 nm.

It is interesting to compare the 1D profiles in Figure 3b with those in the literature referring to the bulk water case. Guido et al.[15] employed a very similar set of CVs to study the ZW stability in a dilute (3 wt %) MEA bulk water solution. In a follow-up study,[16] the same computational methodology was employed to study the capture and release of CO_2 in a 30 wt % MEA bulk water solution. Details of the free-energy profiles and of the chemical mechanism were pretty much identical between the dilute (3 wt %) and concentrated (30 wt %) bulk solution cases: at least up to 30 wt %, the amine concentration does not affect the CO_2 release from the ZW, and (another) MEA in solution did not get directly protonated by ZW deprotonation. The role of water is crucial: it stabilizes the ZW and participates in the proton transfer from the ZW after deprotonation. The equilibrium N–C distance in the ZW is the same in bulk water and at the interface (∼0.16 nm), and also the interfacial barrier for the conversion of ZW into carbamate looks comparable (9 kcal/mol) to the one in bulk water,[15] within the error bar. The only notable difference is the free-energy barrier for the dissociation of the ZW into MEA and CO_2: in bulk water, this barrier is ∼8 kcal/mol,[15] whereas at the interface, it reduces to 4 kcal/mol (Figure 3b, blue line). Free-energy barriers for the 3 and 30 wt % bulk water cases are also reported in Table 1, with the corresponding literature references.

It is worthy to note that the system size employed in this work (1 MEA in 216 water slabs) corresponds to a concentration of ∼1.6 wt %, much lower than those usually

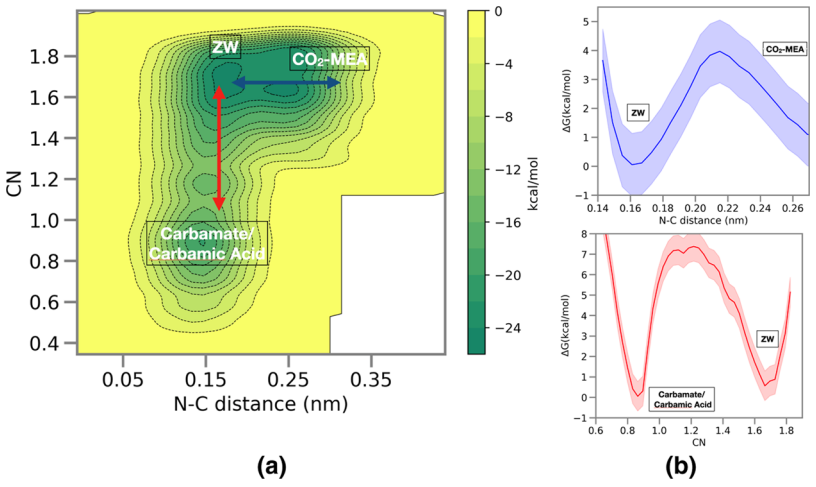

Figure 3. (a) Free-energy landscape as a function of the N–C and CN coordinates for ZW at the air/liquid water interface. (b) Different 1D profiles obtained by umbrella sampling from the metadynamics runs in panel (a). In blue, the 1D profile along the N–C distance is given, and in red, the profile along the CN coordinates is given. The shadow region of the 1D profiles reports the error bar, calculated as block average over the first and last part of the equilibrated umbrella sampling trajectory (details in the SI).

https://doi.org/10.1021/acs.jpcb.1c01661
J. Phys. Chem. B 2021, 125, 4890–4897

Table 1. Free-Energy, Enthalpy, and Entropy Differences at the Different Intermediate States in Bulk Solution (3 and 30 wt % Solutions, refs 15 and 16 Respectively) and at the Interface (This Work)[a]

	bulk			interface			
	ΔG	ΔH	$T\Delta S$	ΔG	ΔH	$T\Delta S$	# HB
CO_2-MEA‡ (S = 1.42)	8[15]	24[15]	16	3 ± 1	12 ± 3	9 ± 3	1.01 ± 0.76
	7[16]	*25*[16]	*18*				
ZW (S = 1.82)	0	0	0	0 ± 1	0 ± 5	0.0 ± 5	2.21 ± 0.93
	0	*0*	*0*				
ZW-Crb‡ (S = 2.10)	8[15]	13[15]	5	9 ± 1	20 ± 5	11 ± 5	3.98 ± 0.94
	9[16]	*12*[16]	*3*				
Carbamate (S = 2.52)	N/A	N/A	N/A	7 ± 1	−7 ± 5	−14 ± 5	4.84 ± 0.89
	∼−7[16]	N/A	N/A				

[a]In italics, values in a 30 wt % bulk solution are given. Consistent with Figure 4a, the ZW is used as a zero reference. Block average analysis has been used to assign error bars. In the last column, the average number of hydrogen bonds between the carboxyl group and water molecules at the interface is given. For the interface case and for each intermediate, values in the table are obtained from statistics over the last 41 ps of FPMD simulations (see SI for further details). A pictorial sketch of the free-energy barrier difference between bulk and interfacial reactions using the values in the table is reported in Figure S4. Energy units in kcal/mol.

employed in industrial processes. However, this is a bulk and not interfacial concentration. Classical MD simulations[25] of a 30 wt % MEA bulk aqueous solution reported an average MEA−water oxygen distance of 0.2−0.3 nm, while the MEA−MEA distance was ∼0.55 nm. This indicates that, even in a 30 wt % solution, the MEA−MEA interaction is water mediated, furthering supporting the statement that, at least up to 30 wt %, the amine concentration does not affect the chemical mechanism.[16] Finally, molecular dynamics of water slabs requires a sufficiently large simulation box to model both the interfacial and bulk regions of the slab. Since FPMD simulations are computationally costly, the simulation box needs to be designed wisely. The standard adopted in many first-principles MD studies of physicochemical processes occurring at the air/water interface[37,38,47] is a slab of ∼216 water molecules with an interfacial area of ∼1.5 × 1.5 nm^2. Here, we decided to solvate one MEA at the air/liquid water interface: adding another (or more) interfacial MEA would have introduced other degrees of freedom (e.g., MEA−MEA distance or MEA−MEA relative orientation), which are difficult to sample in the limited time scale of FPMD simulations and, based on the above considerations, seem (at least in a first approximation) to be irrelevant for the exact details of the chemical pathway.

The main drawback of the N−C and CN coordinates is their inability to accurately discriminate all reaction intermediates in Figure 3. A closer inspection of the metadynamics and umbrella sampling trajectories reveals that the minimum at N−C = ∼1.5 nm and CN = ∼0.9 (Figure 3a) corresponds indeed to the superposition of two very similar structures: the carbamate ion and its protonated form, the carbamic acid. For this reason, we employed a second approach, adopting path CVs based on a recently introduced topological metric.[21] This metric is obtained from a set of coordination numbers among different groups of atoms in the system,[21,44] as described in the methodology section. Here, the advantage is that, taking explicitly into account a rich pattern of multiple coordination and exploiting path CVs (S,Z), the simulation is able to track in detail a variety of complex reaction pathways, also granting the freedom to explore unforeseen ones. The metric for the S,Z space was constructed from three main reaction structures: the reactants, the ZW, and the carbamic acid obtained from the metadynamics run in Figure 3. Figure 4a displays the 2D bias map in the S,Z space obtained from 5.8 ps metadynamics run and starting from the carbamic acid structure. The metadynamics trajectory shows the deprotonation of carbamic acid into carbamate after ∼1 ps. At 2.3 ps, the carbamate converts into the ZW and, at 3.6 ps, CO_2 dissociates from the ZW. No reassociation of the ZW is observed up to the end of the 5.8 ps trajectory. At ∼4.4 ps, MEA protonates, forming $MEAH^+$. Due to the lack of multiple recrossings, this metadynamics run was used only to obtain a description of the chemical pathway in the 2D bias energy landscape defined by the Z and S variables. Compared to Figure 3a, it is possible now to discriminate between carbamate and carbamic acid and to identify an additional structure, i.e., the protonated MEA ($MEAH^+$).

The 2D map in Figure 4 can be refined by umbrella sampling, obtaining a more statistically sampled 1D free-energy profile along the S-coordinate, as shown in Figure 4b. Since amine scrubbing solutions are usually at basic pH conditions, here, also for reasons of computational cost, we focused only on the chemical pathway from the transition barrier of CO_2 release from the ZW (CO_2-MEA‡) up to carbamate. Compared to Figure 3b (where carbamate and carbamic acid were coexisting in the same free-energy minimum), the carbamate ion lies ∼7 kcal/mol above the ZW (Figure 4b), and such a free-energy difference is similar to the (theoretical) pK_a of MEA carbamic acid,[48] explaining the difference between Figures 3b and 4b. The dissociation of the ZW into CO_2 and MEA has a barrier of 3 kcal/mol, whereas this barrier was ∼8 kcal/mol in bulk water.[15] Moreover, the conversion of ZW into carbamate has to overcome a free-energy barrier of ∼9 kcal/mol and the backward reaction is quite facilitated: in fact, the carbamate-to-ZW reaction has a barrier of only 2 kcal/mol. The stability of the carbamate ion is still unclear in a (bulk) aqueous solution: some NMR studies suggested its stability,[49] while other NMR studies did not.[50] Our results indicate that the ZW and carbamate ions are poorly stable at the interface.

The reaction along the S-coordinate in Figure 4b can also be visualized by tracking the charges calculated from a Mulliken population analysis (Figure 4c). In Figure 4c, interacting CO_2 and MEA at S ∼ 1.2 have the CO_2 and NH_2 groups almost neutral (∼±0.2e). As the reaction proceeds, i.e., S increases, the carboxyl and the amine groups become, respectively, more negatively and positively charged. The ZW is formed at S ∼ 1.8, with CO_2 having a −0.6e charge while the NH_2 group having a charge between +0.2e and +0.4e. These charge values

https://doi.org/10.1021/acs.jpcb.1c01661
J. Phys. Chem. B 2021, 125, 4890−4897

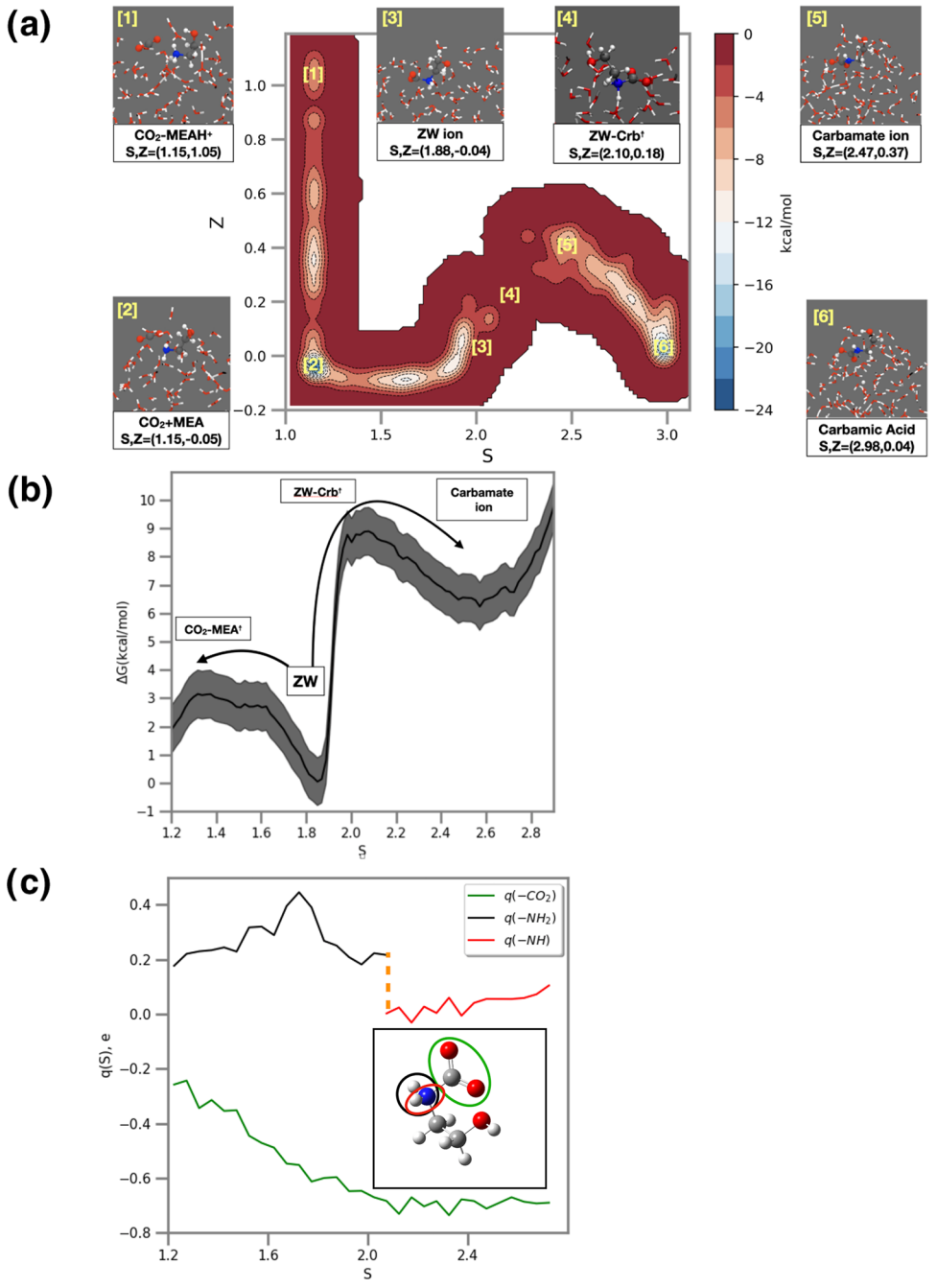

Figure 4. (a) Bias energy landscape in the *S*,*Z* plane for the chemical pathway of ZW at the vapor/liquid water interface. In the insets, the different intermediates observed during the MTD run and their relative position in the *S*,*Z* plane are given. (b) 1D free-energy profile obtained by umbrella sampling along the *S*-coordinate. The shadow region around the profile reports the error bar, calculated as block average over the first and last halves of the equilibrated trajectory from umbrella sampling. (c) Mulliken charges of three different groups, i.e., CO_2, NH_2, and NH, along the reaction coordinate. The vertical dashed orange line marks the change of the amino group by deprotonation, from $-NH_2$ to −NH. N (blue), C (gray), O (red), and H (white).

for the zwitterionic amine and carboxyl group are comparable to those observed in bulk water.[15] In the transition state for the conversion of the ZW into carbamate (ZW-Crb‡) at $S \sim 2.1$, defined as the top of the 1D free-energy profile in Figure 4b, one acidic proton is released from the amine group, which converts into NH. At *S* larger than 2.1, the charge of the amine group drops to zero, while the carboxyl group is $\sim -0.8e$ charged. Those values are a clear sign of the formation of a carbamate singly and negatively charged ion.

The poorer stability of the ZW at the interface compared to the one in bulk solution can be rationalized considering the different solvation environment between the two cases, exploring the enthalpic and entropic contributions to the free-energy barrier for the CO_2 released by interfacial ZW dissociation. This is shown in Table 1 and in Figure S4. In bulk water, the ZW dissociation has an enthalpic barrier of ∼24 kcal/mol:[15] an entropy gain of $T\Delta S$ = 16 kcal/mol was found to be critical in reducing the free-energy barrier of ZW dissociation to ∼8 kcal/mol.[15] In Table 1, we report the

https://doi.org/10.1021/acs.jpcb.1c01661
J. Phys. Chem. B 2021, 125, 4890−4897

enthalpic barriers obtained from the Kohn−Sham energies, using the ZW energy as a zero reference. Enthalpy time series and histograms are reported in Figure S3. Entropic barriers were calculated by subtracting the free-energy barriers from the enthalpic ones. As shown in Table 1, the interfacial enthalpic and $T\Delta S$ barriers for the interfacial dissociation of the ZW into CO_2 and MEA are 12 and 9 kcal/mol, respectively: these values are about half of those recorded in bulk water, i.e., 24 and 16 kcal/mol, respectively. The (half) solvation environment for the ZW at the interface is, therefore, likely responsible for the lower enthalpic barrier. Moreover, the entropic contribution to the interfacial ZW dissociation into CO_2 and MEA is also smaller, as CO_2 is immediately exposed to the gas phase after being released from the ZW, without any significant solvent reorganization. As a result of that, the free-energy barrier, which is the difference of the entropic and enthalpic ones, for ZW dissociation (3 kcal/mol) is about half than that in bulk water (∼8 kcal/mol).[15] Interestingly, the entropic term plays an important role in the interfacial conversion of ZW into carbamate, lowering the free-energy barrier. Indeed, in the ZW-to-carbamate conversion at the interface there is a reorganization of the solvent around the carboxyl group, as suggested by the increase of the average number of H bonds between carboxyl oxygen and water and shown in the last column in Table 1. In the ZW form, the partial charges on the carboxyl atoms are C(0.558e), O(−0.593e), and O(−0.682e), while at the ZW-Crb‡ are C(0.549e), O(−0.710e), and O(−0.800e), with the latter remaining invariant in carbamate. Thus, by deprotonation of the ZW amine group, the carboxyl C−O becomes more polarized, enabling more hydrogen bonding with water and, thus, suggesting an important entropic contribution. Nevertheless, it should be noted that the convergence of enthalpy statistics is difficult due to sizable equilibrium fluctuations (see Figure S3), as also shown by the error bar in Table 1: much longer simulations would be needed to reduce the error bar and to be more assertive on relative enthalpic differences. Finally, we should also note that carbamate lies at a 7 kcal/mol free-energy minimum, while in 30 wt % bulk water, this minimum is ∼−7 kcal/mol (Table 1). This striking difference can be rationalized by the two facts. First, in 30 wt %, the proton released by ZW deprotonation, after being transferred within surrounding water by the Grotthuss mechanism, can protonate another MEA, which could be a more (free energetic) favorable site than water. Second, the computational method used for the 30 wt % bulk water suffers from the same pitfall observed in Figure 3, i.e., the inability to discriminate between the carbamate ion and carbamic acid, artificially lowering the free-energy minimum.

CONCLUSIONS

In this work, we employed a recently developed protocol, which combines a novel topological metric, metadynamics, and umbrella sampling, to investigate the interfacial stability of the monoethanolamine-CO_2 zwitterion. At the vapor/liquid water interface, the monoethanolamine-CO_2 zwitterion is the free-energy minimum structure, but it is poorly stable. Compared to the bulk water case, the (∼half) solvation environment for the interfacial zwitterionic form is responsible for the lower enthalpic and entropic dissociation barriers, almost half of those estimated in bulk, reducing the free-energy barrier for dissociation to ∼3 kcal/mol, from 8 kcal/mol in bulk water. Moreover, the chemical conversion of interfacial ZW into carbamate is hampered by a free-energy barrier of 9 kcal/mol; in turn, carbamate can easily convert back into the zwitterion since the backward barrier is only ∼2 kcal/mol. Altogether, the outcomes of this work strongly point toward the investigation of novel solvents, different from aqueous mixtures, to overcome the limits of the current absorbents. This is especially relevant in the design of cost-effective capture systems at ambient and low CO_2 partial pressures,[11−13] where the capture is likely to occur at the interface of the scrubbing solution.

ASSOCIATED CONTENT

Supporting Information

The Supporting Information is available free of charge at https://pubs.acs.org/doi/10.1021/acs.jpcb.1c01661.

Details of the free-energy settings: description of the N−C and CN reaction coordinates and of the (S,Z) coordinates; umbrella window trajectory in the (S,Z) plane; enthalpic time series; pictorial representation of the free-energy barrier differences for the ZW stability at the interface and in 30 wt % bulk; and input files for PLUMED (PDF)

AUTHOR INFORMATION

Corresponding Author

Ivan Gladich − *Qatar Environment and Energy Research Institute, Hamad Bin Khalifa University, Doha, Qatar;* orcid.org/0000-0003-0929-3439; Email: igladich@hbku.edu.qa

Authors

Alessandro Sinopoli − *Qatar Environment and Energy Research Institute, Hamad Bin Khalifa University, Doha, Qatar*

Ahmed Abotaleb − *Qatar Environment and Energy Research Institute, Hamad Bin Khalifa University, Doha, Qatar*

Fabio Pietrucci − *Sorbonne Université, Muséum National d'Histoire Naturelle, UMR CNRS 7590, IMPMC, 75005 Paris, France;* orcid.org/0000-0002-4892-2667

Complete contact information is available at: https://pubs.acs.org/10.1021/acs.jpcb.1c01661

Notes

The authors declare no competing financial interest.

ACKNOWLEDGMENTS

For HPC resources and services, we acknowledge the Research Computing group in Texas A&M University at Qatar, founded by the Qatar Foundation for Education, Science and Community Development, and a grant from the Computational Materials and Processes Center of the Qatar Environment and Energy Research Institute (CMP-QEERI) under Project No. HPC-P20003. I.G. acknowledges Dr. Marcelo A. Carignano for fruitful discussions.

REFERENCES

(1) Cuéllar-Franca, R. M.; Azapagic, A. Carbon capture, storage and utilisation technologies: A critical analysis and comparison of their life cycle environmental impacts. *J. CO2 Util.* **2015**, *9*, 82−102.

(2) Trachtenberg, M. C.; Bao, L.; Goldman, S. L.; Smith, D. A.; Wu, X. Flue Gas CO2 Capture by a Green Liquid Membrane. In *Greenhouse Gas Control Technologies 7*; Rubin, E. S.; Keith, D. W.; Gilboy, C. F.; Wilson, M.; Morris, T.; Gale, J.; Thambimuthu, K., Eds.; Elsevier Science Ltd: Oxford, 2005; pp 1751−1754.

(3) Markewitz, P.; Kuckshinrichs, W.; Leitner, W.; Linssen, J.; Zapp, P.; Bongartz, R.; Schreiber, A.; Müller, T. E. Worldwide innovations in the development of carbon capture technologies and the utilization of CO2. *Energy Environ. Sci.* **2012**, *5*, 7281−7305.
(4) Maiti, A.; Bourcier, W. L.; Aines, R. D. Atomistic modeling of CO2 capture in primary and tertiary amines − Heat of absorption and density changes. *Chem. Phys. Lett.* **2011**, *509*, 25−28.
(5) Yang, X.; Rees, R. J.; Conway, W.; Puxty, G.; Yang, Q.; Winkler, D. A. Computational Modeling and Simulation of CO2 Capture by Aqueous Amines. *Chem. Rev.* **2017**, *117*, 9524−9593.
(6) Donaldson, T. L.; Nguyen, Y. N. Carbon Dioxide Reaction Kinetics and Transport in Aqueous Amine Membranes. *Ind. Eng. Chem. Fundam.* **1980**, *19*, 260−266.
(7) Xie, H.-B.; He, N.; Song, Z.; Chen, J.; Li, X. Theoretical Investigation on the Different Reaction Mechanisms of Aqueous 2-Amino-2-methyl-1-propanol and Monoethanolamine with CO2. *Ind. Eng. Chem. Res.* **2014**, *53*, 3363−3372.
(8) Ghezloun, A.; Saidane, A.; Oucher, N.; Chergui, S. The Post-Kyoto. *Energy Procedia* **2013**, *36*, 1−8.
(9) Abotaleb, A.; El-Naas, M. H.; Amhamed, A. Enhancing gas loading and reducing energy consumption in acid gas removal systems: A simulation study based on real NGL plant data. *J. Nat. Gas Sci. Eng.* **2018**, *55*, 565−574.
(10) Luis, P. Use of monoethanolamine (MEA) for CO2 capture in a global scenario: Consequences and alternatives. *Desalination* **2016**, *380*, 93−99.
(11) Shi, X.; Xiao, H.; Azarabadi, H.; Song, J.; Wu, X.; Chen, X.; Lackner, K. S. Sorbents for the Direct Capture of CO2 from Ambient Air. *Angew. Chem., Int. Ed.* **2020**, *59*, 6984−7006.
(12) Elfving, J.; Bajamundi, C.; Kauppinen, J. Characterization and Performance of Direct Air Capture Sorbent. *Energy Procedia* **2017**, *114*, 6087−6101.
(13) Fujikawa, S.; Selyanchyn, R.; Kunitake, T. A new strategy for membrane-based direct air capture. *Polym. J.* **2021**, *53*, 111−119.
(14) Gladich, I.; Abotaleb, A.; Sinopoli, A. Tuning CO2 Capture at the Gas/Amine Solution Interface by Changing the Solvent Polarity. *J. Phys. Chem. B* **2020**, *124*, 10245−10256.
(15) Guido, C. A.; Pietrucci, F.; Gallet, G. A.; Andreoni, W. The Fate of a Zwitterion in Water from ab Initio Molecular Dynamics: Monoethanolamine (MEA)-CO2. *J. Chem. Theory Comput.* **2013**, *9*, 28−32.
(16) Ma, C.; Pietrucci, F.; Andreoni, W. Capture and Release of CO2 in Monoethanolamine Aqueous Solutions: New Insights from First-Principles Reaction Dynamics. *J. Chem. Theory Comput.* **2015**, *11*, 3189−3198.
(17) Ma, C.; Pietrucci, F.; Andreoni, W. Reaction dynamics of $$ \hbox {CO}_2$$CO2in aqueous amines from ab initio molecular dynamics: 2-amino-2-methyl-1,3-propanediol (AMPD) compared to monoethanolamine (MEA). *Theor. Chem. Acc.* **2016**, *135*, No. 60.
(18) Hwang, G. S.; Stowe, H. M.; Paek, E.; Manogaran, D. Reaction mechanisms of aqueous monoethanolamine with carbon dioxide: a combined quantum chemical and molecular dynamics study. *Phys. Chem. Chem. Phys.* **2015**, *17*, 831−839.
(19) Xie, H.-B.; Zhou, Y.; Zhang, Y.; Johnson, J. K. Reaction Mechanism of Monoethanolamine with CO2 in Aqueous Solution from Molecular Modeling. *J. Phys. Chem. A* **2010**, *114*, 11844−11852.
(20) Shim, J.-G.; Kim, J.-H.; Jhon, Y. H.; Kim, J.; Cho, K.-H. DFT Calculations on the Role of Base in the Reaction between CO2 and Monoethanolamine. *Ind. Eng. Chem. Res.* **2009**, *48*, 2172−2178.
(21) Pietrucci, F.; Saitta, A. M. Formamide reaction network in gas phase and solution via a unified theoretical approach: Toward a reconciliation of different prebiotic scenarios. *Proc. Natl. Acad. Sci. U.S.A.* **2015**, *112*, 15030.
(22) Melnikov, S. M.; Stein, M. Molecular Dynamics Study of the Solution Structure, Clustering, and Diffusion of Four Aqueous Alkanolamines. *J. Phys. Chem. B* **2018**, *122*, 2769−2778.
(23) Huang, I.-S.; Li, J.-J.; Tsai, M.-K. Solvation Dynamics of CO2(g) by Monoethanolamine at the Gas−Liquid Interface: A Molecular Mechanics Approach. *Molecules* **2017**, *22*, No. 8.
(24) Melnikov, S. M.; Stein, M. Solvation and Dynamics of CO2 in Aqueous Alkanolamine Solutions. *ACS Sustainable Chem. Eng.* **2019**, *7*, 1028−1037.
(25) Melnikov, S. M.; Stein, M. The effect of CO2 loading on alkanolamine absorbents in aqueous solutions. *Phys. Chem. Chem. Phys.* **2019**, *21*, 18386−18392.
(26) da Silva, E. F.; Kuznetsova, T.; Kvamme, B.; Merz, K. M. Molecular Dynamics Study of Ethanolamine as a Pure Liquid and in Aqueous Solution. *J. Phys. Chem. B* **2007**, *111*, 3695−3703.
(27) Ma, C.; Pietrucci, F.; Andreoni, W. Capturing CO2 in Monoethanolamine (MEA) Aqueous Solutions: Fingerprints of Carbamate Formation Assessed with First-Principles Simulations. *J. Phys. Chem. Lett.* **2014**, *5*, 1672−1677.
(28) Bougie, F.; Pokras, D.; Fan, X. Novel non-aqueous MEA solutions for CO2 capture. *Int. J. Greenhouse Gas Control* **2019**, *86*, 34−42.
(29) Zhou, S.; Nguyen, B. T.; Richard, J. P.; Kluger, R.; Gao, J. Origin of Free Energy Barriers of Decarboxylation and the Reverse Process of CO2 Capture in Dimethylformamide and in Water. *J. Am. Chem. Soc.* **2021**, *143*, 137−141.
(30) Marx, D.; Hutter, J. *Ab Initio Molecular Dynamics*; Cambridge University Press: New York, 2009.
(31) Hutter, J.; Iannuzzi, M.; Schiffmann, F.; VandeVondele, J. cp2k: atomistic simulations of condensed matter systems. *Wiley Interdiscip. Rev.: Comput. Mol. Sci.* **2014**, *4*, 15−25.
(32) Becke, A. D. Density-functional exchange-energy approximation with correct asymptotic behavior. *Phys. Rev. A* **1988**, *38*, 3098−3100.
(33) Lee, C.; Yang, W.; Parr, R. G. Development of the Colle-Salvetti correlation-energy formula into a functional of the electron density. *Phys. Rev. B* **1988**, *37*, 785−789.
(34) Grimme, S.; Antony, J.; Ehrlich, S.; Krieg, H. A consistent and accurate ab initio parametrization of density functional dispersion correction (DFT-D) for the 94 elements H-Pu. *J. Chem. Phys.* **2010**, *132*, No. 154104.
(35) Goedecker, S.; Teter, M.; Hutter, J. Separable dual-space Gaussian pseudopotentials. *Phys. Rev. B* **1996**, *54*, 1703−1710.
(36) Jones, A.; Leimkuhler, B. Adaptive stochastic methods for sampling driven molecular systems. *J. Chem. Phys.* **2011**, *135*, No. 084125.
(37) Baer, M. D.; Mundy, C. J.; McGrath, M. J.; Kuo, I. F. W.; Siepmann, J. I.; Tobias, D. J. Re-examining the properties of the aqueous vapor−liquid interface using dispersion corrected density functional theory. *J. Chem. Phys.* **2011**, *135*, No. 124712.
(38) Kathmann, S. M.; Kuo, I. F. W.; Mundy, C. J.; Schenter, G. K. Understanding the Surface Potential of Water. *J. Phys. Chem. B* **2011**, *115*, 4369−4377.
(39) Gladich, I.; Chen, S.; Vazdar, M.; Boucly, A.; Yang, H.; Ammann, M.; Artiglia, L. Surface Propensity of Aqueous Atmospheric Bromine at the Liquid−Gas Interface. *J. Phys. Chem. Lett.* **2020**, *11*, 3422−3429.
(40) Jorgensen, W. L.; Chandrasekhar, J.; Madura, J. D.; Impey, R. W.; Klein, M. L. Comparison of simple potential functions for simulating liquid water. *J. Chem. Phys.* **1983**, *79*, 926−935.
(41) Gladich, I.; Habartová, A.; Roeselová, M. Adsorption, Mobility, and Self-Association of Naphthalene and 1-Methylnaphthalene at the Water−Vapor Interface. *J. Phys. Chem. A* **2014**, *118*, 1052−1066.
(42) Gladich, I.; Abotaleb, A.; Sinopoli, A. Tuning CO2 Capture at the Gas/Amine Solution Interface by Changing the Solvent Polarity. *J. Phys. Chem. B* **2020**, *124*, 10245−10256.
(43) Bonomi, M.; Bussi, G.; Camilloni, C.; Tribello, G. A.; Banáš, P.; Barducci, A.; Bernetti, M.; Bolhuis, P. G.; Bottaro, S.; Branduardi, D.; Capelli, R.; Carloni, P.; Ceriotti, M.; Cesari, A.; Chen, H.; Chen, W.; Colizzi, F.; De, S.; De La Pierre, M.; Donadio, D.; Drobot, V.; Ensing, B.; Ferguson, A. L.; Filizola, M.; Fraser, J. S.; Fu, H.; Gasparotto, P.; Gervasio, F. L.; Giberti, F.; Gil-Ley, A.; Giorgino, T.; Heller, G. T.; Hocky, G. M.; Iannuzzi, M.; Invernizzi, M.; Jelfs, K. E.; Jussupow, A.; Kirilin, E.; Laio, A.; Limongelli, V.; Lindorff-Larsen, K.; Löhr, T.; Marinelli, F.; Martin-Samos, L.; Masetti, M.; Meyer, R.; Michaelides,

https://doi.org/10.1021/acs.jpcb.1c01661
J. Phys. Chem. B 2021, 125, 4890−4897

A.; Molteni, C.; Morishita, T.; Nava, M.; Paissoni, C.; Papaleo, E.; Parrinello, M.; Pfaendtner, J.; Piaggi, P.; Piccini, G.; Pietropaolo, A.; Pietrucci, F.; Pipolo, S.; Provasi, D.; Quigley, D.; Raiteri, P.; Raniolo, S.; Rydzewski, J.; Salvalaglio, M.; Sosso, G. C.; Spiwok, V.; Šponer, J.; Swenson, D. W. H.; Tiwary, P.; Valsson, O.; Vendruscolo, M.; Voth, G. A.; White, A.; The, Pc. Promoting transparency and reproducibility in enhanced molecular simulations. *Nat. Methods* **2019**, *16*, 670−673.

(44) Laporte, S.; Pietrucci, F.; Guyot, F.; Saitta, A. M. Formic Acid Synthesis in a Water−Mineral System: Major Role of the Interface. *J. Phys. Chem. C* **2020**, *124*, 5125−5131.

(45) Laio, A.; Parrinello, M. Escaping free-energy minima. *Proc. Natl. Acad. Sci. U.S.A.* **2002**, *99*, 12562.

(46) Kumar, S.; Rosenberg, J. M.; Bouzida, D.; Swendsen, R. H.; Kollman, P. A. Multidimensional free-energy calculations using the weighted histogram analysis method. *J. Comput. Chem.* **1995**, *16*, 1339−1350.

(47) Zhu, C.; Kais, S.; Zeng, X. C.; Francisco, J. S.; Gladich, I. Interfaces Select Specific Stereochemical Conformations: The Isomerization of Glyoxal at the Liquid Water Interface. *J. Am. Chem. Soc.* **2017**, *139*, 27−30.

(48) Jackson, P.; Beste, A.; Attalla, M. Insights into amine-based CO2 capture: an ab initio self-consistent reaction field investigation. *Struct. Chem.* **2011**, *22*, 537−549.

(49) Lv, B.; Guo, B.; Zhou, Z.; Jing, G. Mechanisms of CO2 Capture into Monoethanolamine Solution with Different CO2 Loading during the Absorption/Desorption Processes. *Environ. Sci. Technol.* **2015**, *49*, 10728−10735.

(50) Barzagli, F.; Mani, F.; Peruzzini, M. A 13C NMR study of the carbon dioxide absorption and desorption equilibria by aqueous 2-aminoethanol and N-methyl-substituted 2-aminoethanol. *Energy Environ. Sci.* **2009**, *2*, 322−330.

https://doi.org/10.1021/acs.jpcb.1c01661
J. Phys. Chem. B 2021, 125, 4890−4897